Spring 2017

Effect of Sintering Temperature on Microstructure, Corrosion Behavior, and Hardness of Nanocrystalline Al-5at.%Ni and Al-5at.%V Alloys

Matthew G. Wachowiak
University of Akron, mgw21@zips.uakron.edu

Effect of Sintering Temperature on Microstructure, Corrosion Behavior and Hardness of Nanocrystalline Al-5at.%Ni and Al-5at.%V Alloys

4250:497

Author: Matthew Wachowiak

Advisor: Dr. Rajeev Gupta

Readers: Dr. Scott Lillard, Dr. Qixin Zhou

Spring 2017

Executive Summary

Purpose

Aluminum alloys are commonly used because of their high strength to weight ratio. More corrosion resistant aluminum alloys are of great interest to nearly every industry that currently utilizes aluminum alloys. Unfortunately, the alloying elements form secondary phases which cause significant decreases in corrosion resistance. It has been shown recently that high-energy ball milled Al-transition metal alloys showed high strength and corrosion resistance[1-3]. Thermal stability of the high-energy ball milled alloys is not well understood. The purpose of this project was to investigate thermal stability of high energy ball milled Al-5at.%Ni and Al-5at.%V by varying sintering temperature. Of particular interest are hardness and corrosion properties. These are affected by the microstructure; especially solid solubility, intermetallics, and grain size.

Results

Hardness of Al-5at.%Ni and Al-5at.%V alloys was measured as a function of sintering temperature. For Al-5at.%Ni, Vickers hardness decreased from 249.6 (±5.75) for an unsintered sample, to 87.2 (±6.63) upon sintering at 614 °C. For Al-5at.%V, the hardness for an unsintered sample was about 271.7 (±7.67), decreasing to 133.0 (±6.6) after sintering at 614 °C. Reported hardness values are averages based on averages of 5 repetitions, each of which had a standard deviation less than 10 Vickers hardness number, and values for each test are shown in appendix A. The grain sizes of the unsintered Al-5at. %Ni and Al-5at.%V were 35.0 nm and 35.5nm respectively which, increased to 4890 nm for Al-5at.%Ni and 1440 nm for Al-5at.%V upon sintering at 614 °C . Solid solubility of Ni decreased from 2 at.% (unsintered) to 9.7×10^{-7} at.% due to sintering at 614 °C. Solid solubility of vanadium began at about 3 at.% and decreased to

.017 at.% for the 614 °C sample. Corrosion behavior of the two alloys was also influenced by the sintering temperature. Al-5at.%Ni samples displayed no transition potentials, whereas Al-5at.%V displayed transition potentials for the lower sintering temperature samples. Both samples had weak correlations between sintering temperature and pitting potential, but there was a tendency for pitting potential to decrease for higher sintering temperatures in both alloys. There was a decrease in corrosion current as sintering temperature increased for Al-5at.%Ni and corrosion current was relatively consistent for Al-5at.%V.

Conclusions

Hardness testing, scanning electron microscopy (SEM) and x-ray diffraction (XRD) resulted in several findings related to the mechanical properties and microstructure of the alloys tested. Microstructure, corrosion behavior and hardness were significantly influenced by the sintering temperature. SEM showed that the alloys became less porous as sintering temperature was increased. Grain size and solid solubility were also determined using X-ray diffraction analysis and correlated with the hardness and corrosion properties. Cyclic potentiodynamic polarization (CPP) was used to evaluate the corrosion properties of the alloys. There was, however; a direct correlation between the pitting potential of the alloys and Vickers hardness, which relates to an inverse relationship between pitting potential and sintering temperature.

Implications of Work

These results can be of benefit to society as a basis for approaches to developing more corrosion resistant aluminum alloys. This work will be used as a starting point for further research in the development of such alloys. My work on this project introduced me to laboratory techniques that were previously unfamiliar to me. High energy ball milling, cold compaction, hardness testing,

and cyclic potentiodynamic polarization (CPP) were all processes that I had no prior experience with. I had some prior exposure to SEM, EDX, and XRD, but not the opportunity to use them in broader application. This is also the first formal lab research I have conducted, so it gave me the opportunity to experience this side of corrosion prevention. The work also helped to give me more confidence in my ability to work in that kind of setting. This work will be continued by a graduate student, who will present a paper on the subject at Materials Science and Technology 2017 conference, Pittsburgh, PA.

Recommendations

It is recommended that further testing be done on these and other aluminum alloys. Specifically, additional polarization tests to generate more reproducible results. In this project, only one sample was tested for each sintering temperature, so testing of additional samples is recommended. My recommendation to students working on similar projects is to always ask questions and to ask for help if it is needed. There will always be professors and graduate students around that would be more than happy to answer questions or recommend better lab practices.

Introduction and Background

Pure aluminum possesses good corrosion resistance but low strength, so alloying elements are often added to increase strength. Limited solubility of the most of the alloying elements in Al leads to the formation of secondary phases which are detrimental to corrosion [1,4,5]. The strength of many Al alloys is based on precipitation hardening, which depends upon precipitation of secondary phases. Because of this, high-strength Al alloys are reported to exhibit poor corrosion resistance[1,4-6]. Recent research has reported that in addition to composition of the secondary phases, size, shape, number, and distribution of the secondary phases play important role in corrosion of Al alloys[6-7]. Corrosion behavior and hardness can be optimized by using suitable processing methods and composition[8].

Research has been conducted to create stronger and more corrosion resistant aluminum alloys by high-energy ball milling and various alloying elements[2,3,9]. The research focused on studying the effect of high-energy ball milling on Al-Cr alloys, which resulted in significant improvement in corrosion properties over cast alloys and pure aluminum[2-3]. Similarly, ongoing research has shown significant improvement in corrosion resistance and hardness due to high-energy ball milling and alloying with V and Ni. The improvement in corrosion resistance and strength has been attributed to grain refinement to less than 100 nm and solid solubility increased to well beyond the thermodynamic solubility[10]. High-energy ball milling represent a metastable state therefore decomposition of supersaturated solid solution to more stable phases and grain growth during high temperature exposure are real possibilities[10]. Understanding the thermal stability of these alloys is of paramount interest to determine the processing temperature and properties during service conditions.

The objective of this project was to investigate the effect of sintering temperature on microstructure, hardness and corrosion properties of Al-5at.%Ni and Al-5at.%V. Thermal stability of the alloys largely depends upon the diffusion coefficients of the alloying elements. Therefore, vanadium and nickel were used in this study due their different diffusion coefficients in Al. For example, at 400 °C, diffusion coefficients for Vanadium and Ni in Al have been reported to be on the order of 10^{-23} and 10^{-14} respectively[10]. This research will help to better understand thermal stability of high energy ball milled aluminum alloys.

Experimental Methods

Sample Preparation

Samples were prepared via high-energy ball milling followed by cold compaction, and then sintering. Ball milling was done using 99.7% purity aluminum powder of size -50/+100 mesh and 99.8% purity alloying elements of size -100 mesh. The powder was combined and placed in steel jars with a 16:1 ball-to-powder ratio by weight for 100 hours at 280 RPM with a 30 minute rest period for every hour of milling. The jars contained stearic acid as a process controlling agent. The powder was then consolidated using an auto pellet press in a tungsten carbide die under uniaxial pressure. The final pressure of 3 GPa was held for ten minutes. For sintering, the furnace was set to the appropriate temperature and allowed stabilize for one hour after reaching the desired temperature. The samples were then placed in the furnace for one hour. Sintering temperatures began at 100 °C and increased in increments of 100 °C. 450 °C was also included because significant changes near that temperature range were expected. 614°C was chosen as a temperature near the melting point of the alloy, but not high enough to risk melting parts of the sample.

Sample Characterization

Vickers hardness was measured using a Wilson Tukon 1202 Vickers hardness tester. A 25 g load was applied with a 10 second dwelling time for the indenter. For each sample, 5 repetitions were completed; also ensuring the standard deviation was below 10. The samples were polished up to 0.05 μm diamond suspension, and ultrasonic cleaning in ethanol was done for 5 minutes. A Tescan Lyra 3 FIB-FESEM in back scatter electron mode with an accelerating voltage of 20 kV was used to collect scanning electron microscope (SEM) images. At least 5 point scans were done using energy dispersive x-ray spectroscopy (EDXS). X-ray diffraction (XRD) was done under Cu K-α radiation (λ=0.1541nm) with a 10-90° 2θ range, 1 °/min scan rate, and a .01° step size.

Corrosion Testing

Samples were mounted in epoxy and polished to 1200 grit SiC sandpaper before each cyclic potentiodynamic polarization (CPP). The tests were done in flat mount cells, with a platinum mesh counter electrode and a saturated calomel reference electrode (SCE). The solution used was 0.01 M NaCl. For each test, the open circuit potential (OCP) was monitored for 20 minutes to ensure it was steady before beginning the polarization. CPP was completed 2-3 times for each sample.

Data and Results

Figures 1 and 2 show the SEM images at 500x magnification for Al-5at.%Ni and Al-5at.%V, respectively. Figures 3 and 5 show the SEM images at 20,000x magnification for Al-5at.%Ni and Al-5at.%V, respectively. For Al-5at.%Ni, the 500 times magnification images show what appears to be a progressive decrease in porosity. The same is true for Al-5at.%V, but it is less

pronounced. Both alloys have darker and lighter sections. The darker parts are the aluminum matrix, and the lighter spots are the precipitates. This is only really visible in the 20,000 times magnification images. Evolution of intermetallic phases with increasing temperature is clearly visible in the two alloys. Sintering at 614 °C showed coarse rod like intermetallics in Al-5at.%V whereas spherical particles were observed in Al-5at. %Ni

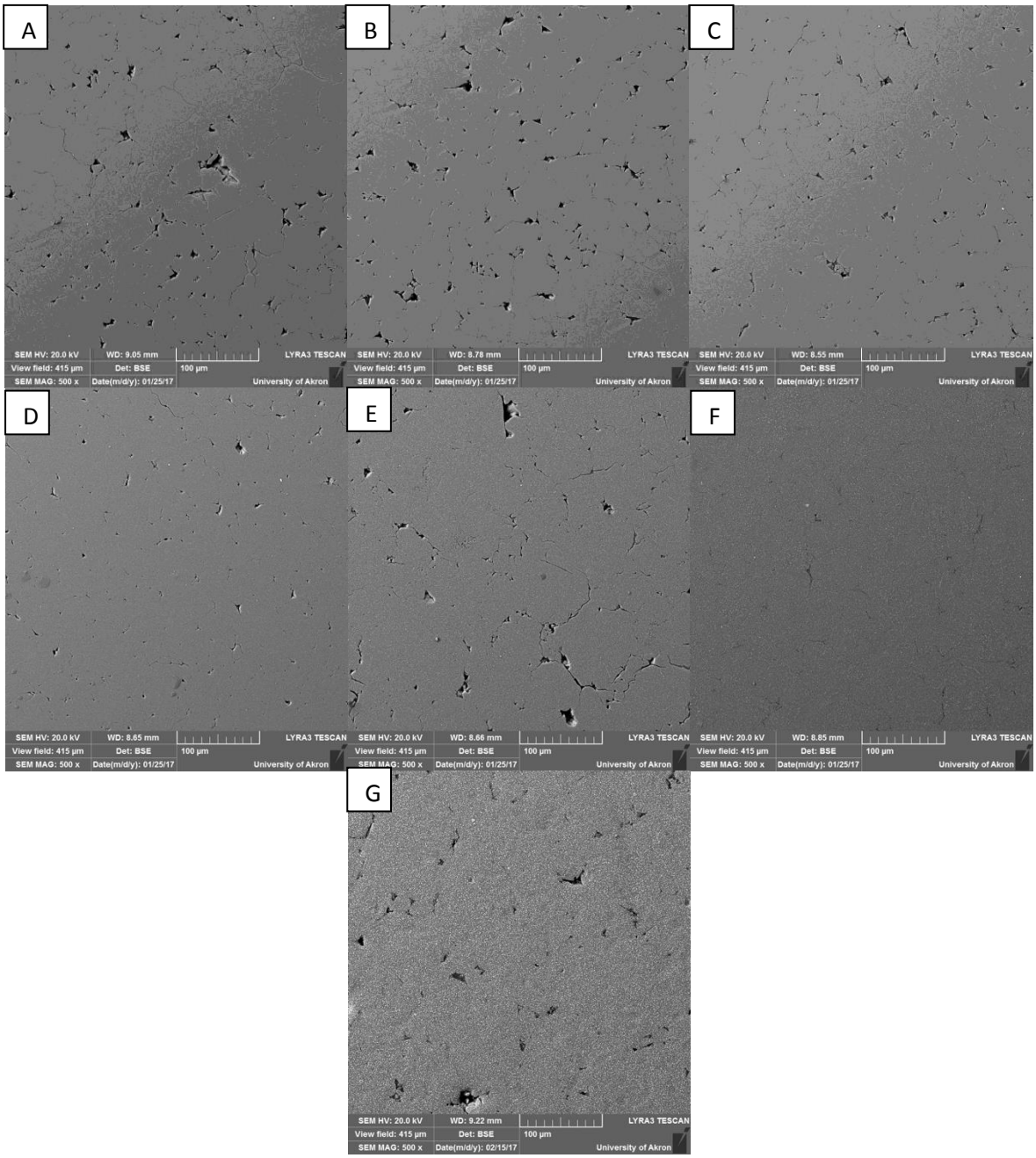

Figure 1: Back scatter electron SEM images of Al-5at.%Ni at 500x magnification sintered at (A): 100°C, (B): 200°C, (C): 300°C, (D): 400°C, (E): 450°C, (F): 500°C (G): 614°C

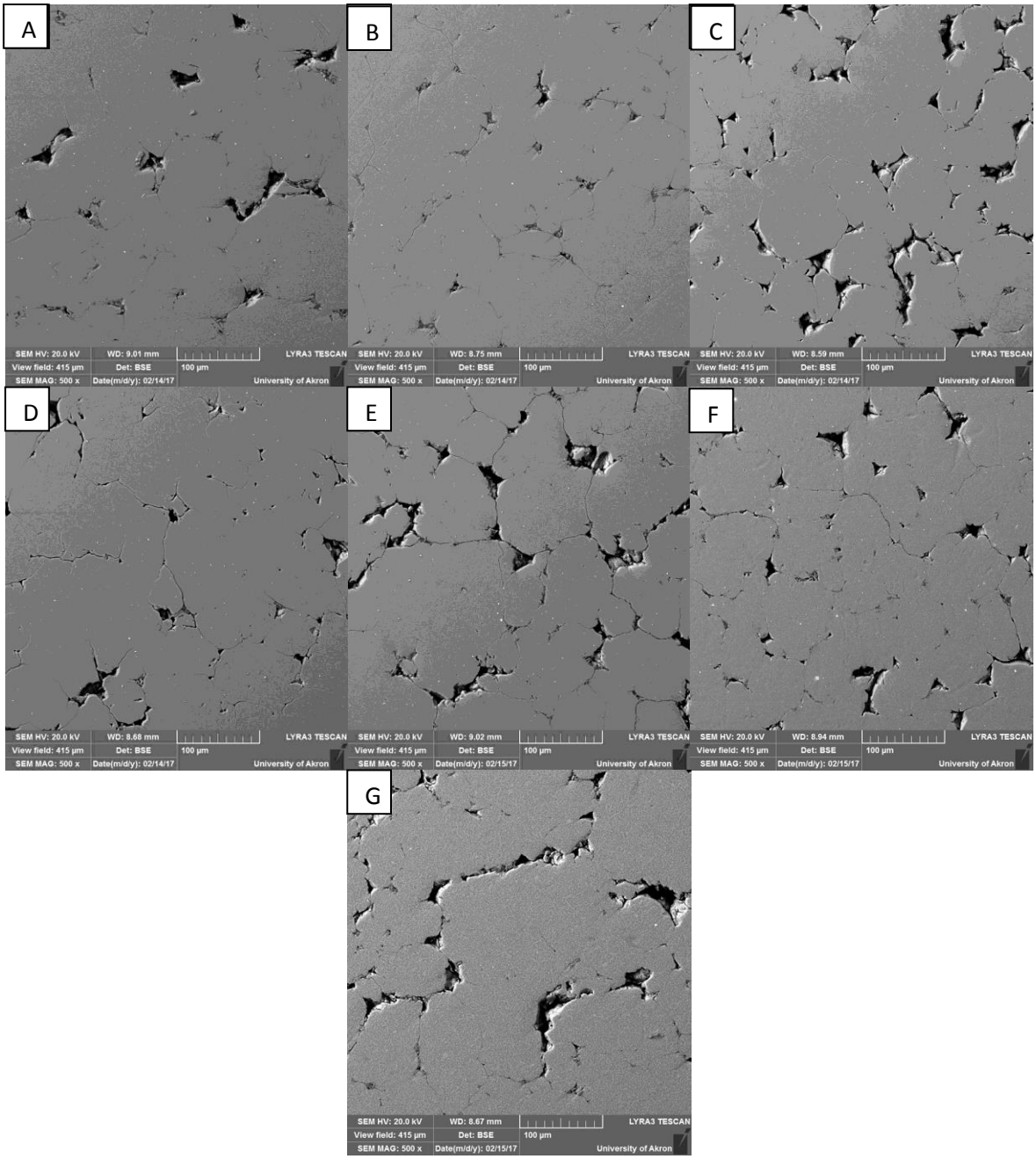

Figure 2: Back scatter electron SEM images of Al-5at.%V at 500x magnification sintered at (A): 100°C, (B): 200°C, (C): 300°C, (D): 400°C, (E): 450°C, (F): 500°C (G): 614°C

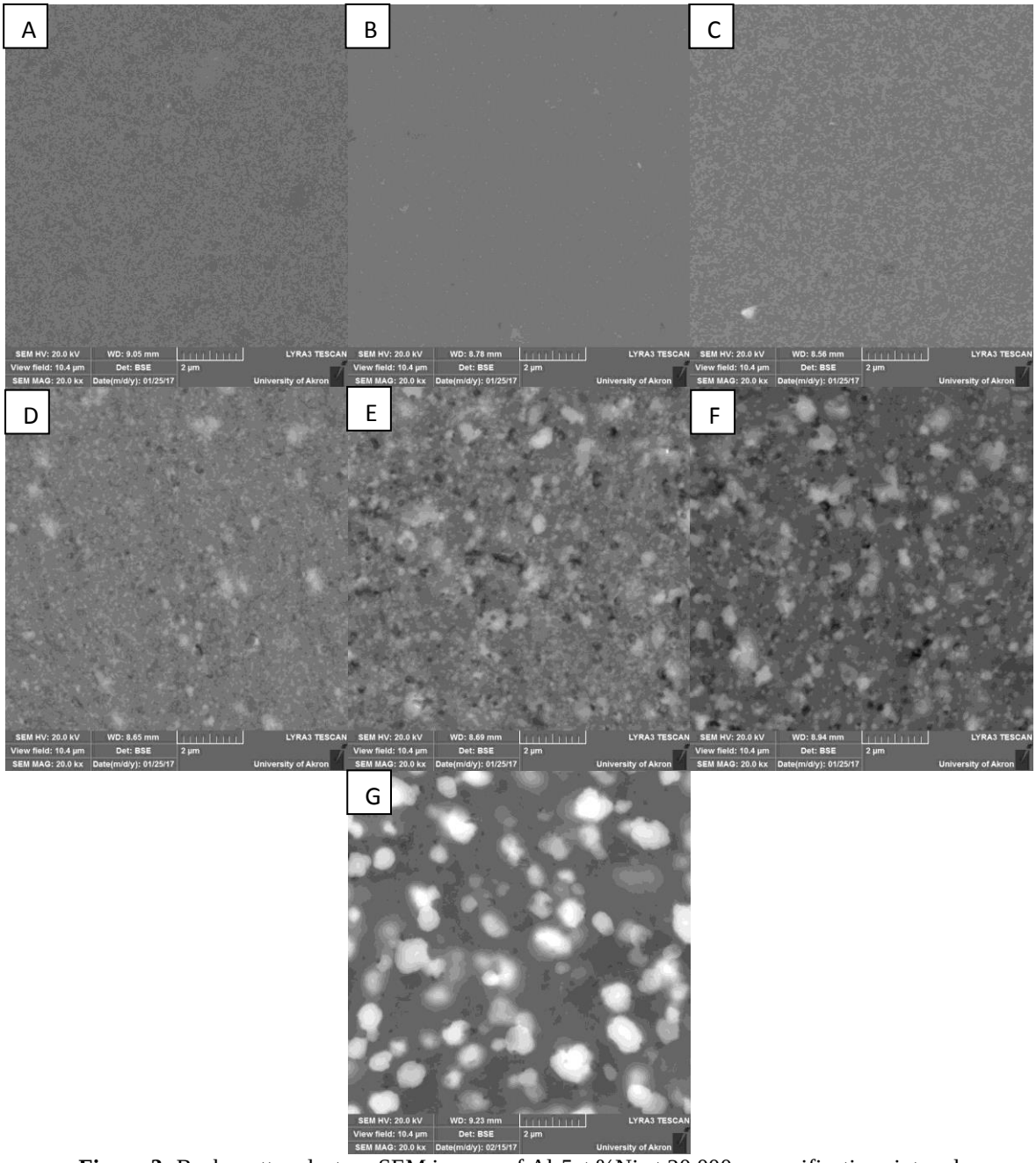

Figure 3: Back scatter electron SEM images of Al-5at.%Ni at 20,000x magnification sintered at (A): 100°C, (B): 200°C, (C): 300°C, (D): 400°C, (E): 450°C, (F): 500°C (G): 614°C

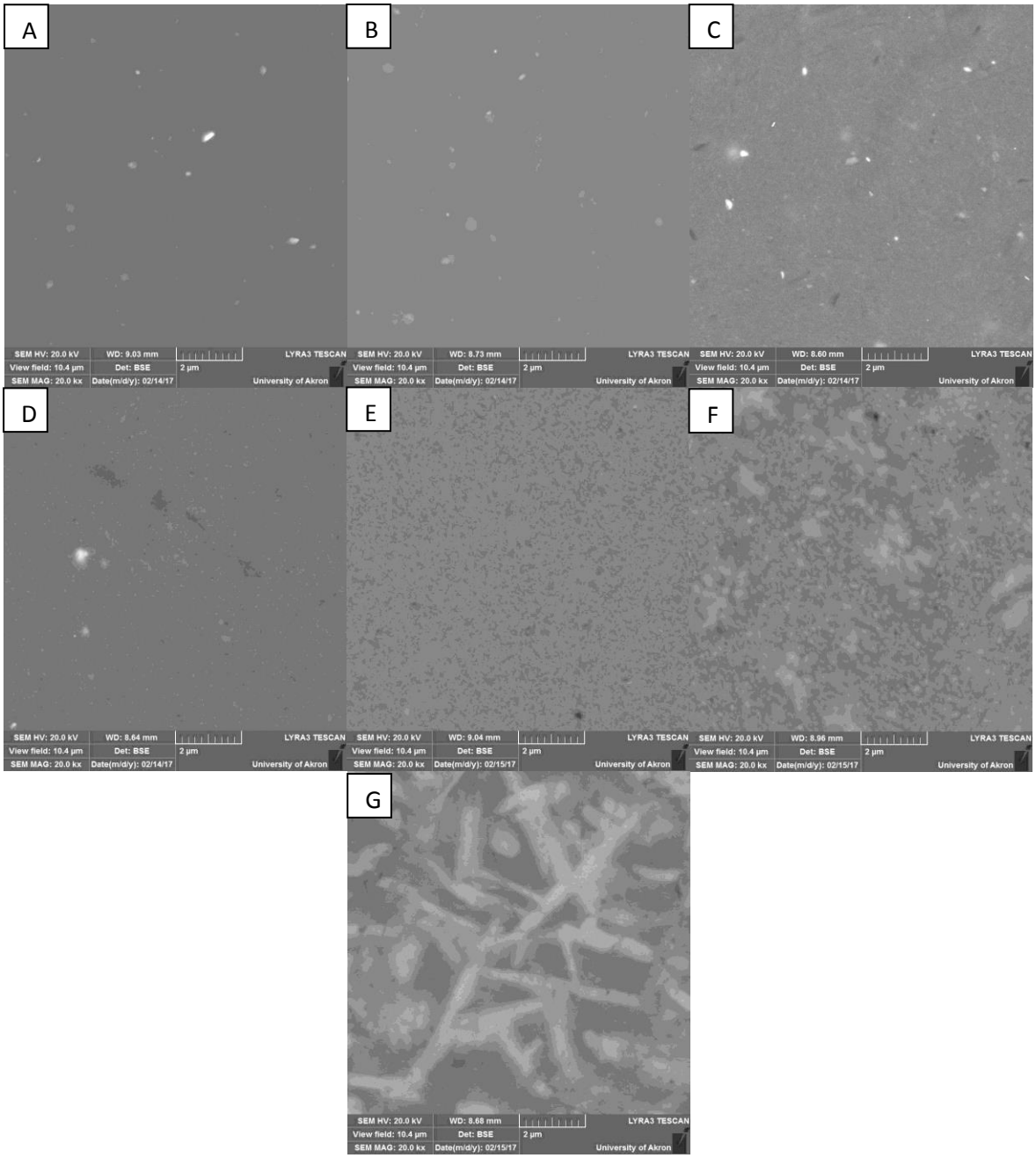

Figure 4: Back scatter electron SEM images of Al-5at.%V at 20,000x magnification sintered at (A): 100°C, (B): 200°C, (C): 300°C, (D): 400°C, (E): 450°C, (F): 500°C (G): 614°C

Figures 5 and 6 show the XRD scans for Al-5at.%Ni and Al-5at.%V, respectively. Both contain the full spectrum scan and a close-up view of the primary peak. Peaks corresponding Ni or V do not appear in XRD scan indicating complete alloying. Additional peaks corresponding to intermetallics appear in Al-5at.%Ni upon sintering at 300 °C. Al-5at.%V show higher thermal

stability, intermetallic peaks appear after 400 °C. High thermal stability of Al-5at.%V can be attributed to significantly lower diffusivity of V. Narrower peaks indicate grain growth, and the peak shifts can indicate changes in solid solubility. Peaks became narrower with increasing the sintering temperature. The single peak charts show a shift to the left as temperature increases, which coincides with a decrease in solid solubility.

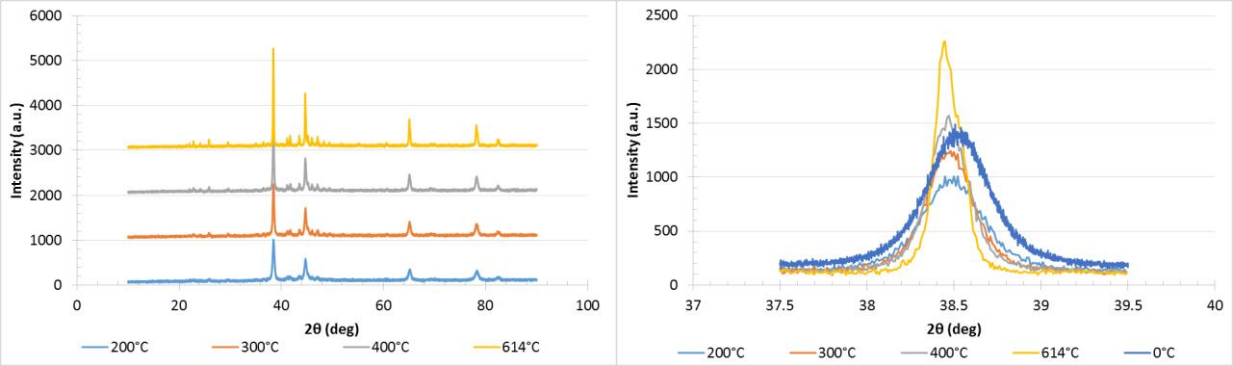

Figure 5: (left): full XRD scans for Al-5at.%Ni, (right): Primary peak of XRD scans for Al-5at.%Ni

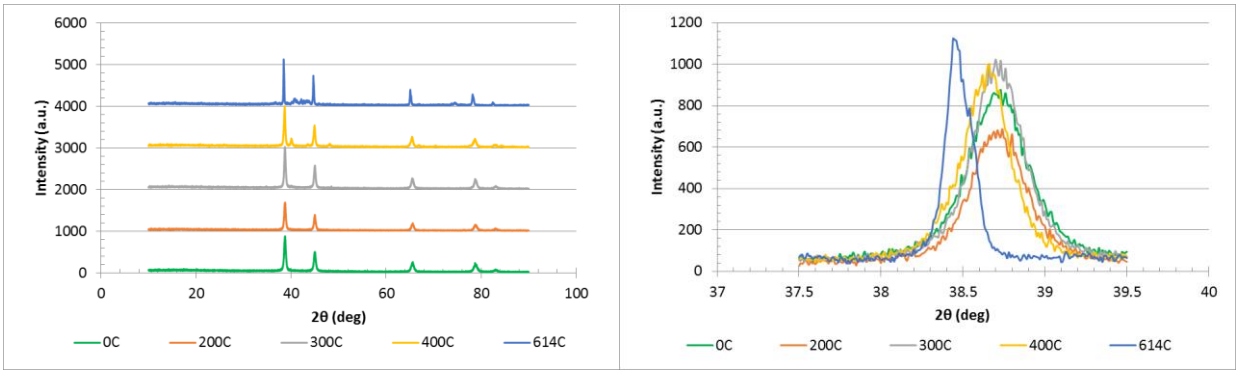

Figure 6: (left): full XRD scans for Al-5at.%V, (right): Primary peak of XRD scans for Al-5at.%V

Figure 7 illustrates the effect of sintering temperature on both grain size and solid solubility. Grain size increases nearly exponentially with sintering temperature. For Al-5at.%V, solid solubility is steady until 400 °C where it has decreased significantly. This is in contrast with Al-5at.%Ni, which decreases steadily throughout the sintering temperature range. Error bars were excluded from all plots for clarity.

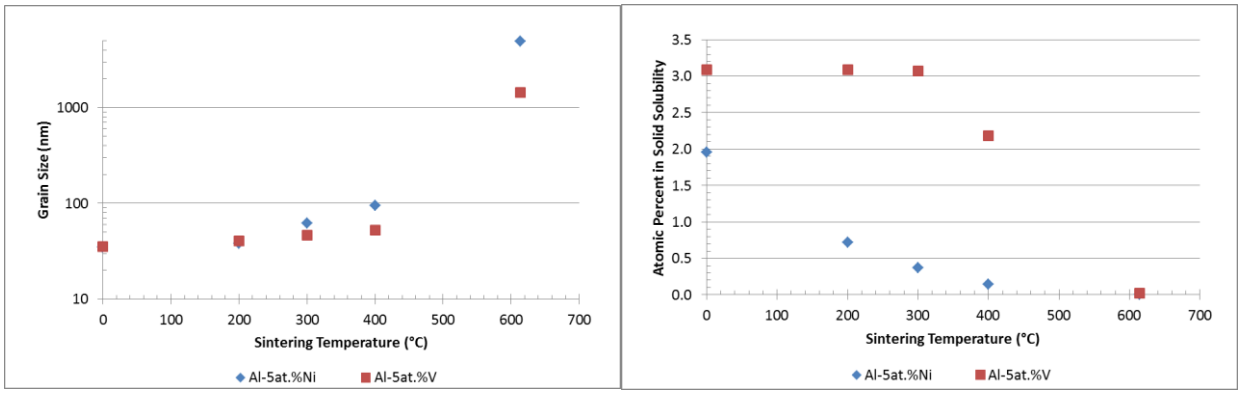

Figure 7: (Left): Grain size and (right): Atomic percent in solid solubility as functions of sintering temperature for Al-5at.%Ni and Al-5at.%V

Figures 8 and 9 show the CPP curves for Al-5at.%Ni and Al-5at.%V, respectively, at each sintering temperature. Only one curve for each temperature is included to facilitate viewing. Pitting potentials and transition potentials were read of the graphs, and corrosion current was calculated using the tafel fit analysis tool built in the EC-Lab software used. Appendix B contains the raw data from the polarization tests.

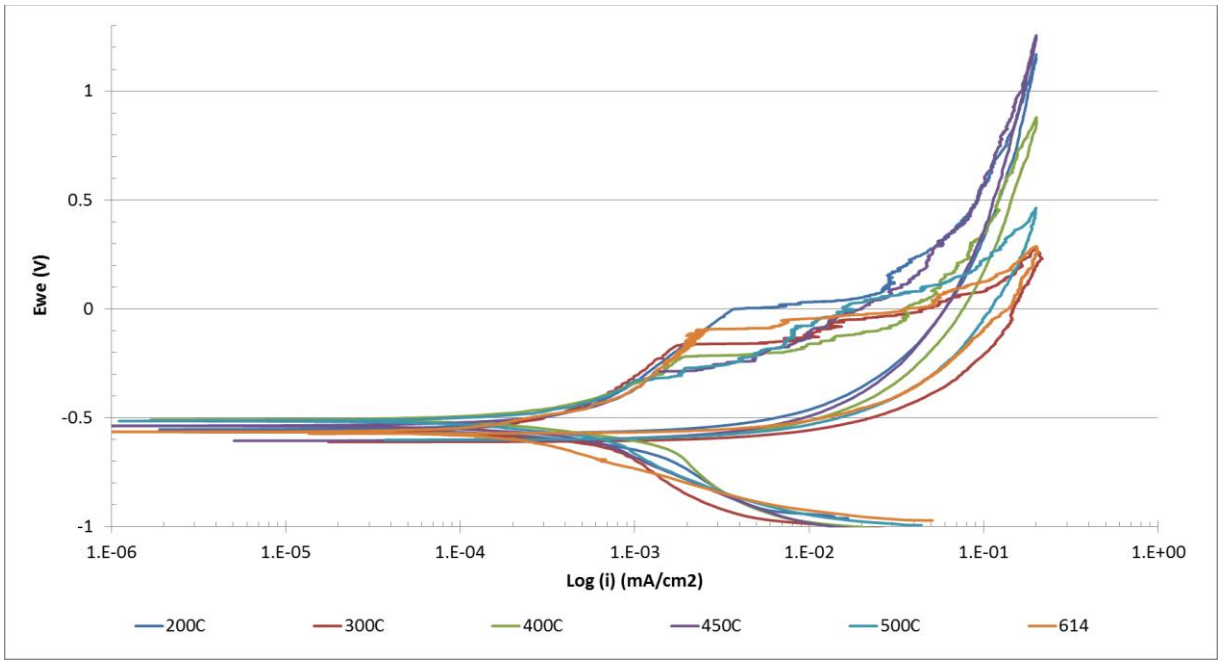

Figure 8: Cyclic potentiodynamic polarization curves for Al-5at.%Ni at various sintering temperatures

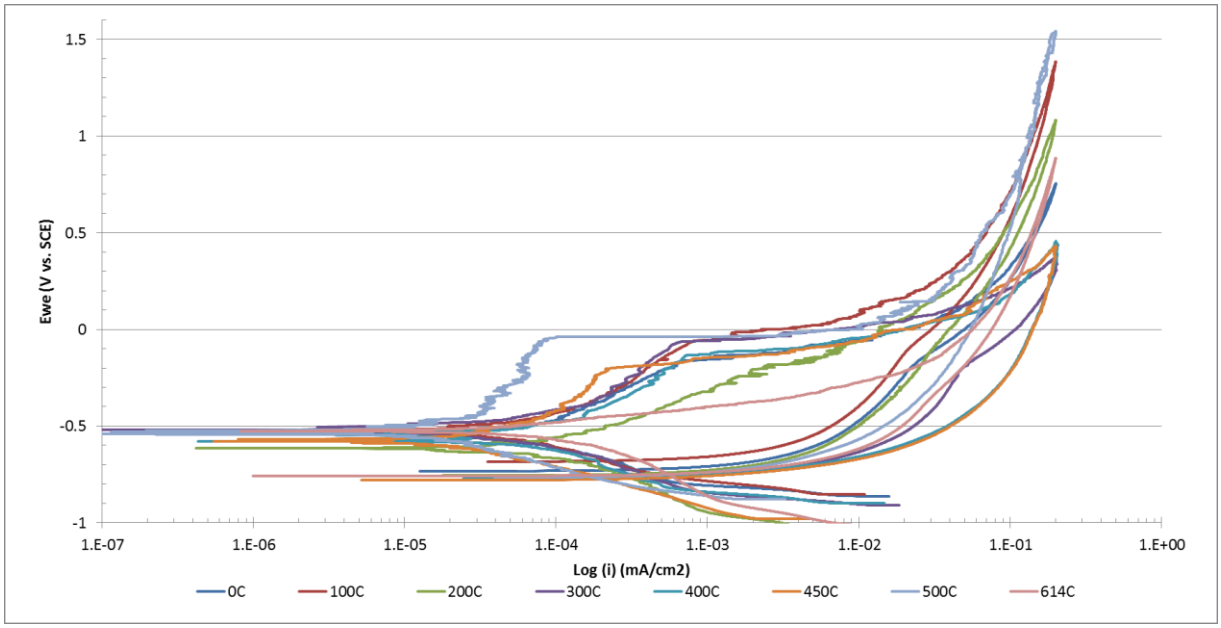

Figure 9: Cyclic potentiodynamic polarization curves for Al-5at.%V at various sintering temperatures

Figure 10 shows an example of a single CPP curve with labeled pitting potential, transition potential, and corrosion current. Pitting potential was identified by locating the point where the slope decreases drastically. The transition potential was identified by locating the characteristic change of inflection. The method for finding corrosion current was mentioned above.

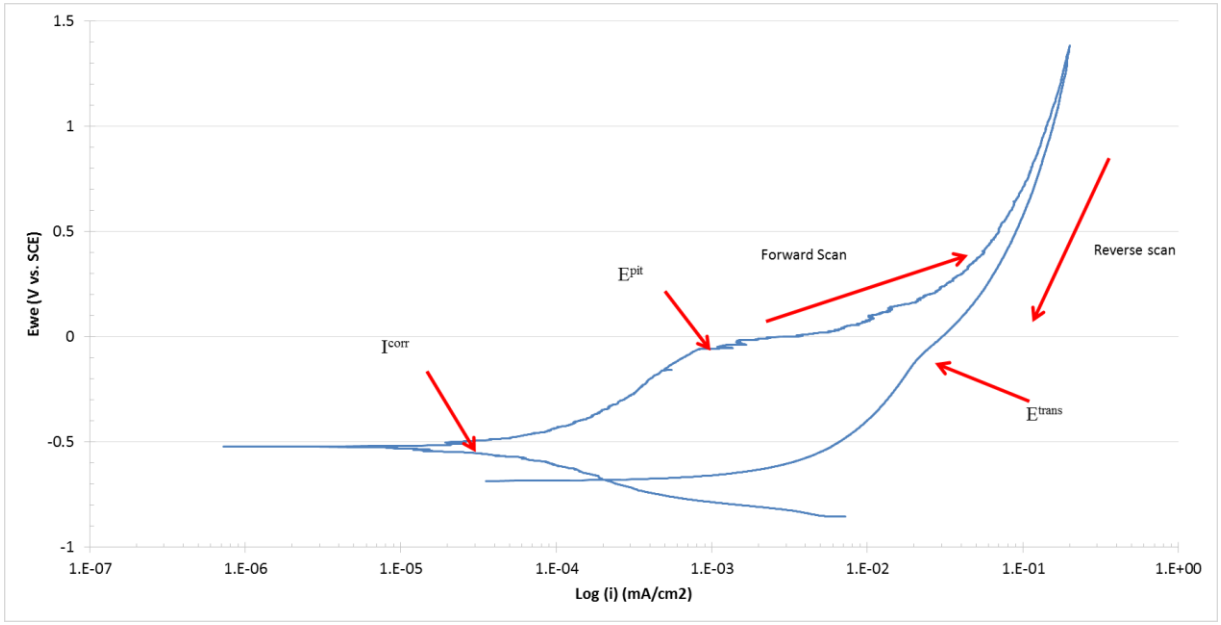

Figure 10: Cyclic potentiodynamic polarization curve for Al-5at.%V sintered at 100°C with labels to indicate points of interest

Figure 11 shows the relationship between the corrosion properties and sintering temperature. For Al-5at.%Ni, the general trend is a decrease in pitting potential and corrosion current as sintering temperature increases. For Al-5at.%V, corrosion current and transition potential appear to be relatively consistent over the full range of temperatures. Pitting potential also appears to be relatively consistent, until dropping appreciably at higher temperatures. Al-5at.%V sintered at 200 °C shows a higher transition potential than pitting potential.

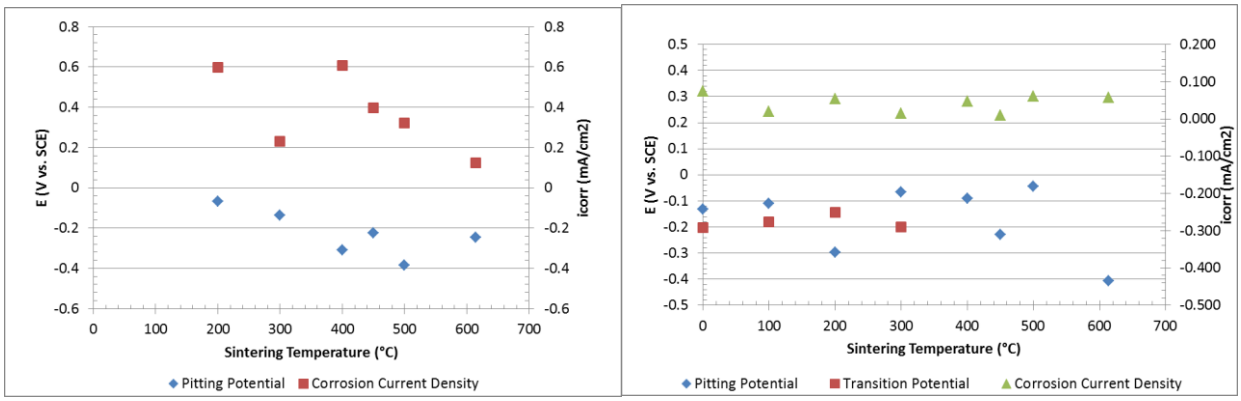

Figure 11: Pitting potential, transition potential, and corrosion current as functions of sintering temperature for (left): Al-5at.%Ni and (right): Al-5at. %V

Figure 12 shows the decrease in hardness as sintering temperature increases. The hardness of Al-5at.%V increases until 200°C. This is presumably a result of precipitation hardening, the effect of which decreases at the higher sintering temperatures.

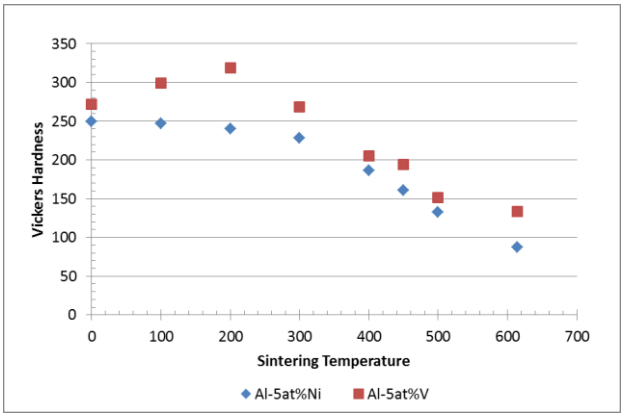

Figure 12: Vickers hardness as a function of sintering temperature for Al-5at.%Ni and Al-5at.%V

Figure 13 illustrates the effect of grain size and solid solubility on hardness. Hardness decreases as grain size increases for both alloys; the relationship is similar for both alloys. Hardness and solid solubility have a direct relationship for both alloys, but it is logarithmic for Al-5at.%Ni and exponential for Al-5at.%V.

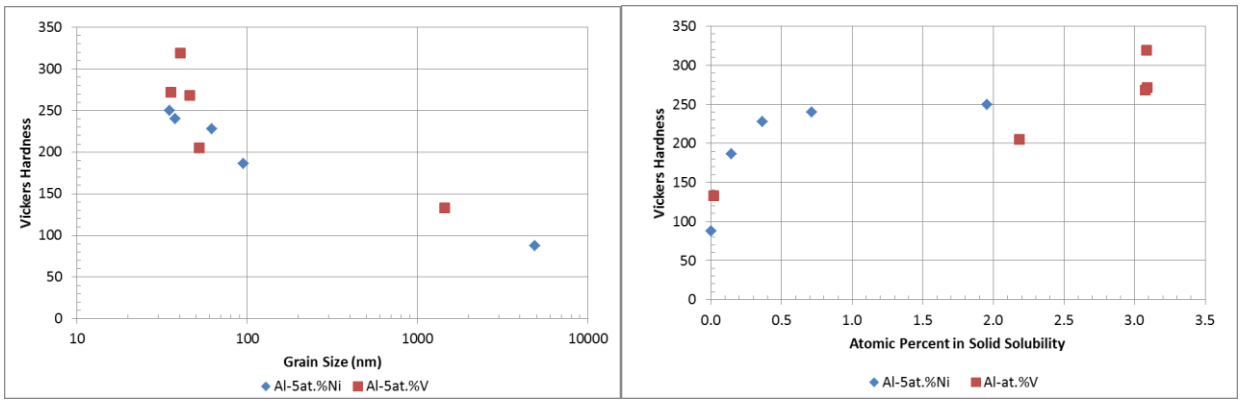

Figure 13: Vickers hardness as a function of (left): grain size and (right): atomic percent in solid solubility for Al-5at.%Ni and Al-5at.%V

Figure 14 shows the pitting potentials, transition potentials, and the corrosion current as functions of grain size. There appears to be little correlation, with the exception of a decrease in pitting potential as grain size increases for Al-5at.%Ni.

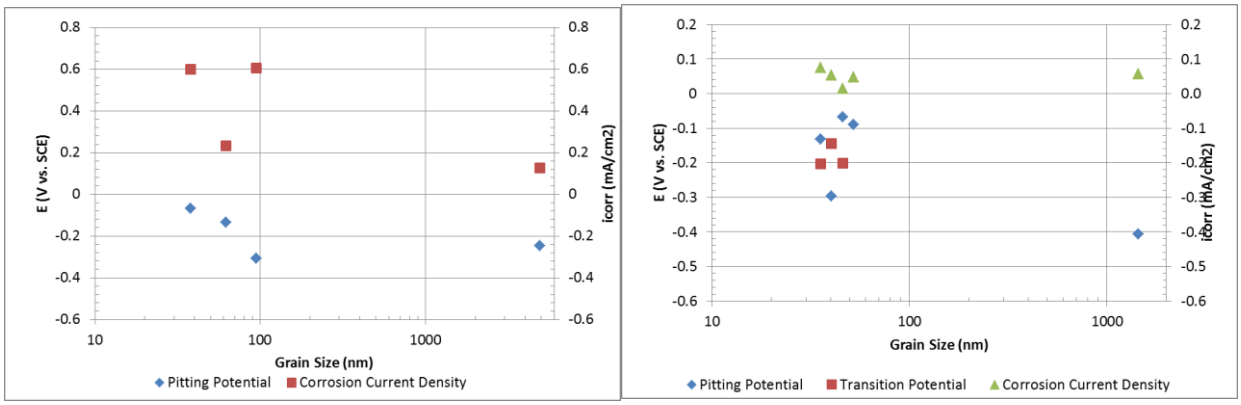

Figure 14: Pitting potential, transition potential, and corrosion current as functions of grain size for (left): Al-5at.%Ni and (right): Al-5at.%V

Figure 15 shows the pitting potentials, transition potentials, and corrosion current as functions of solid solubility. There appears to be little correlation for Al-5at.%V, but for Al-5at.%Ni, corrosion current density increases with pitting potential.

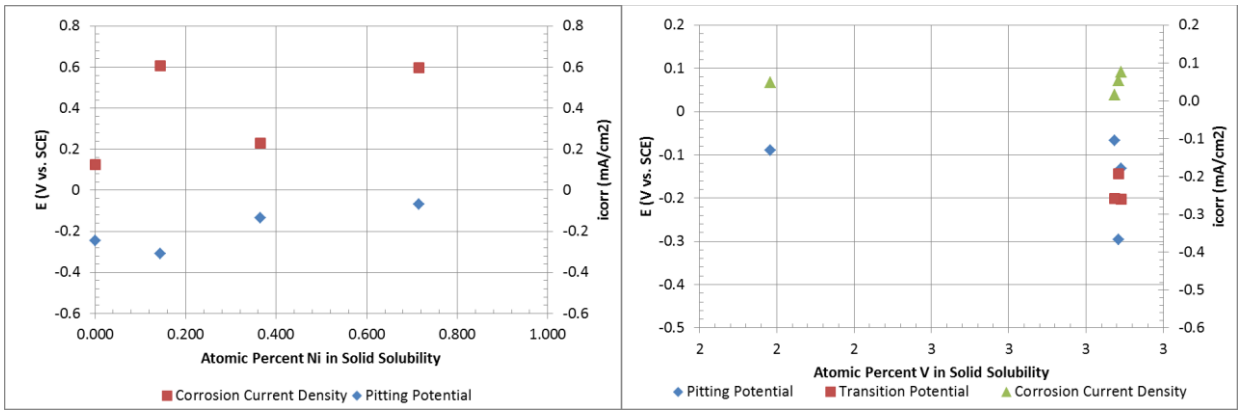

Figure 15: Pitting potential, transition potential, and corrosion current as functions of atomic percent of alloying elements in solid solubility for (left): Al-5at.%Ni and Al-5at.%V

Figure 16 shows pitting potential as a function of hardness for both alloys. Al-5at.%Ni shows a slight correlation between the two, whereas Al-5at.%V is more difficult to assess. The highest pitting potential was achieved at 200 °C for Al-5at.%Ni, and at 500 °C for Al-5at.%V. The highest hardness was achieved at 100 °C for Al-5at.%Ni and at 200 °C for Al-5at.%V

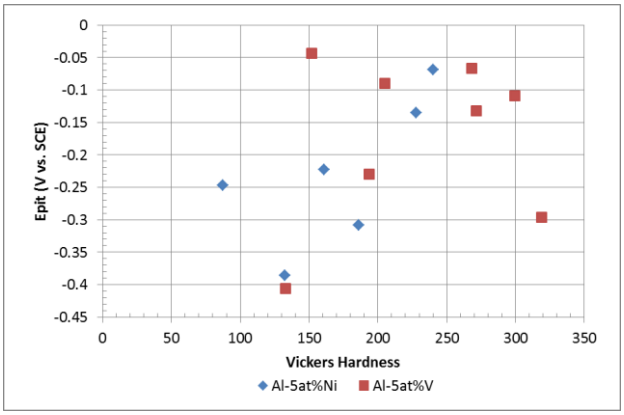

Figure 16: Pitting potential as a function of hardness for Al-5at.%Ni and Al-5at.%V

Discussion and Analysis

The results above indicate that sintering temperature has an effect on mechanical properties. An increase in sintering temperature showed an increase in grain size and a decrease in solid solubility. These results explain the decrease in hardness as sintering temperature increases. The grain sizes at 614°C were each above 1000 nm, which is outside the accurate range of the XRD analysis technique. EDX scans showed the expected compositions, and were not included due to the availability of XRD analysis. EDX showed small amounts of chromium and iron in the samples. This is likely from the stainless steel balls used in high energy ball milling, and could be a source of error.

Al-5at.%V showed little correlation between the sintering temperature and the corrosion properties, but Al-5at.%Ni showed a decrease in both corrosion current and pitting potential as sintering temperature increased. It is important to note, however; that only 2-3 repetitions of CPP were performed for each sample due to time constraints. There were some complications in mounting the samples relating to achieving adequate connection from the potentiostat to the sample. This is believed to be primarily related to the adhesive on the copper tape used. This can also explain the noise in some of the curves, as well as the inverted pitting and transition potentials for Al-5at.%V at 200°C. It is recommended that additional CPP experiments be and that multiple samples be sintered for each temperature for reproducibility.

Acknowledgements

I would like to thank Javier Esquivel for taking SEM images, performing EDX and XRD analysis, and for helping me in the lab.

Literature Cited

[1] Esquivel, J., Gupta, R. K. (2017) Corrosion behavior and hardness of Al-m (M: Mo, Si, Ti, Cr) alloys. *Acta Metall. Sin (Engl Lett), 30* (4), 333-341

[2] Gupta, R. K., Fabijanic, D., Zhang, R., Birbilis, N. (2015) Corrosion behavior and hardness of in situ consolidated nanostructured Al and Al-Cr alloys produced via high-energy ball milling. *Corrosion science, 98,* 643-650

[3] Gupta, R. K., Fabijanic, D., Dorin, T., Qiu, Y., Wang, J. T., Birbilis, N. (2015) Simultaneous improvement in the strength and corrosion resistance of Al via high-energy ball milling and Cr alloying. *Materials and Design, 84,* 270-276

[4] Polmear, I., John, D. S. (2005) Light alloys: from traditional alloys to nanocrystals. *Butterworth-Heinemann*

[5] Gupta, R. K., Zhang, R., Davies, C. H. J., Birbilis, N. (2014) A theoretical study of the influence of microalloying on sensitization of AA5083 and moderation of sensitization via Sr additions, *Corrosion, 70 (402)*

[6] Gupta, R. K., Xia, L.J. Zhou, X., Sha, G., Gun, B., Ringer, S.P., Birbilis, N., (2015) Corrosion behavior of Al-4Mg-1Cu (wt%) microalloyed with Si and Ag, *Advanced Engineering Materials, 17 (1670)*

[7] Gupta, R. K., Deschamps, A., Cavanaugh, M. K., Lynch, S.P., Birbilis, N. (2012) Relating the early evolution of microstructure with electrochemical response and mechanical performance of Cu rich and Cu lean 7xxx aluminum alloys. *Journal of the Electrochemical Society, 159 (C492)*

[8] Esquivel, J., Gupta, R.K., (2016) Simultaneous improvement of corrosion and mechanical properties of aluminum alloys. *Light Metals* 151

[9] Gupta, R. K., Murty, B. S., Birbilis, N. an overview of High-energy ball milled nanocrystalline aluminum alloys. (2017) *SpringerBriefs in Materials*

[10] Knipling, K. E., Dunand, D. C., Seidman, D. N. (2006) Criteria for developing castable, creep-resistant aluminum-based alloys- a review. *Z. Metallkd, 97 (3),* 246-265

Appendix A: Hardness Testing Raw Data

Al-5at.%5Ni							
Temperature	100	200	300	400	450	500	614
1	246.3	243.7	226.1	192.5	161.5	128.9	75.7
2	260.4	243.7	233.4	183.5	173.6	135.2	91
3	246.3	235.9	223.8	183.5	175.2	133.1	88.7
4	246.3	249	228.5	185.3	142	127.9	88.1
5	235.9	228.5	228.5	185.3	152	137.4	92.3
STDEV	8.72	8.02	3.57	3.73	14.16	4.06	6.63
AVG	247.04	240.16	228.06	186.02	160.86	132.5	87.16
Al-5at.%V							
Temperature	100	200	300	400	450	500	614
1	299.3	318.2	260.3	200.2	190.6	157.3	128.9
2	299.3	326.3	263.3	206.2	187	154.6	133
3	303	318.2	269.3	204.2	188.8	150.6	124.9
4	310.4	314.3	278.8	206.2	200.2	149.4	142
5	285.4	318.2	269.3	208.3	202.1	146.8	136.3
Avg	299.48	319.04	268.2	205.02	193.74	151.74	133.02
STDEV	9.082	4.396	7.092	3.060	6.916	4.191	6.601

Appendix B: Polarization and Mechanical Average Values

Al-5at.%Ni							
Sintering Temperature (°C)	E^{pit}	E^{trans}	E^{corr}	I^{corr}	Vickers Hardness	Solid Solubility	Grain Size
0					249.6	1.956	34.977
100					247.04		
200	-0.0690		-0.548	0.598	240.16	0.715	37.766
300	-0.1350		-0.516	0.231	228.06	0.365	61.848
400	-0.3087		-0.522	0.606	186.02	0.145	94.886
450	-0.2230		-0.567	0.396	160.86		
500	-0.3860		-0.603	0.3215	132.5		
614	-0.2465		-0.533	0.1255	87.16	0.000	4886.554

Al-5at.%V							
Sintering Temperature (°C)	E^{pit}	E^{trans}	E^{corr}	I^{corr}	Vickers Hardness	Solid Solubility	Grain Size
0	-0.13165	-0.203	-0.546	0.075	271.667	3.091	35.527
100	-0.10925	-0.181	-0.467	0.020	299.48		
200	-0.296	-0.1445	-0.527	0.054	319.04	3.084	40.362
300	-0.0671	-0.201	-0.519	0.015	268.2	3.075	46.093
400	-0.0895		-0.556	0.048	205.02	2.183	52.378
450	-0.2296		-0.522	0.010	193.74		
500	-0.0433		-0.590	0.061	151.74		
614	-0.4065		-0.531	0.057	133.02	0.017	1439.610